LOCAL VELOCITY POSTPROCESSING FOR MULTIPOINT FLUX METHODS ON GENERAL HEXAHEDRA

MARY WHEELER, GUANGRI XUE, AND IVAN YOTOV

Abstract. The authors formulated in [32] a multipoint flux mixed finite element method that reduces to a cell-centered pressure system on general quadrilaterals and hexahedra for elliptic equations arising in subsurface flow problems. In addition they showed that a special quadrature rule yields $\mathcal{O}(h)$ convergence for face fluxes on distorted hexahedra. Here a first order local velocity postprocessing procedure using these face fluxes is developed and analyzed. The algorithm involves solving a 3×3 system on each element and utilizes an enhanced mixed finite element space introduced by Falk, Gatto, and Monk [18]. Computational results verifying the theory are demonstrated.

Key Words. mixed finite element, multipoint flux approximation, cell-centered finite difference, mimetic finite difference, full tensor coefficient, quadrilaterals, hexahedra, postprocessing.

1. Introduction

A major motivation for defining accurate locally conservative numerical methods for elliptic equations with tensor coefficients is the increasing interest in the modeling of subsurface flow and transport in porous media. Subsurface systems or geosystems may be natural, such as aquifers and fossil fuel reservoirs, or artificial, such as landfills and nuclear waste sites and are seen today as resources that must be managed. Geosystems are complex, however, for they involve multiple physical and chemical processes operating across multiple spans of time (from nanoseconds to centuries) and space (from nanometers to kilometers) and involve highly varying heterogeneities.

Effective management of a geosystem must be based on conceptual and numerical models of the geosystem. An important example of geosystem applications is CO_2 sequestration, which is the long-term isolation of carbon dioxide from the atmosphere in geological reservoirs. Geologic sequestration by injection of CO_2 into deep brine aquifers and reservoirs represents one of the most promising approaches for reducing the increases in atmospheric CO_2, which have been blamed for recent trends in global warming and alarming changes in weather patterns. The basis for this potential is the huge global storage capacity existing in geologic formations and the availability and close proximity of potential injection sites to power generation
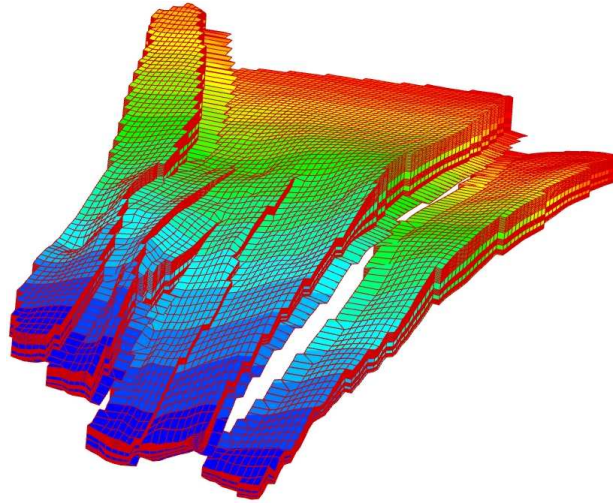
FIGURE 1. Hexahedral meshes in Frio CO_2 demonstration site

plants. Another example is the disposal of nuclear wastes. The safe disposal of nuclear waste in geologic media is a complex problem that requires extensive modeling and simulation to assess the long-term performance of the disposal system. The calculations have to address the response of the site over thousands of years and incorporate multiscale and multiphysics coupling to various extents depending on the geologic medium. Predictive computational simulation is essential for providing the information needed to make decisions on site selection, design, and operation of repositories long before the repository response can be measured. In addition, uncertainty quantification will play a major part in the modeling and simulation of the repository response. Other examples include methane gas migration, bioremediation, management of groundwater systems, geothermal systems, increasing oil and gas production, and CO_2 injection for enhanced oil and gas recovery.

Although each geosystem mentioned above has its unique physics that require site-specific models, all geosystem models will have at their base certain general capabilities to which site-specific capabilities can be added. These general capabilities include multiscale and multiphysics models and numerical algorithms for approximating the pertinent physical, chemical, geological, and biological processes characteristic of these systems. Effective modeling of geosystems necessitates the formulation of accurate and efficient locally conservative algorithms for computing velocities and pressures on general grids [16, 13]. Using hexahedra involves fewer degrees of freedom than tetrahedral grids and can accurately represent geological layers as shown in Figure 1, the Frio CO_2 demonstration site. In addition, as discussed above, geosystem models involve modeling different processes such as diffusion/dispersion and reactive transport and thus requiring accurate velocities within elements and on faces. Examples include parabolic equations, streamline methods, and using higher order discontinuous Galerkin approximations for transport.

Here we consider multipoint flux mixed finite element (MFMFE) discretizations for Darcy flow on general hexahedral grids. The method is motivated and closely related to the multipoint flux approximation (MPFA) method [1, 2, 15, 14]. In the MPFA finite volume formulation, sub-edge (sub-face) fluxes are introduced, which allows for local flux elimination and reduction to a cell-centered scheme.

Similar elimination is achieved in the MFMFE variational framework, by employing appropriate finite element spaces and special quadrature rules. Our approach is based on the BDM_1 [8] in 2D or the $BDDF_1$ [7] and CD_1 [11] spaces in 3D with a trapezoidal quadrature rule applied on the reference element. This approach allows for rigorous analysis of the numerical error [34, 20, 32, 29, 33] for simplicial, quadrilateral, hexahedral, and triangular prismatic grids. A related formulation based on a broken Raviart-Thomas space is developed in [21, 22] on quadrilaterals.

A major difficulty in MFE approximations on hexahedra is due to the fact that standard velocity spaces such as the lowest order Raviart-Thomas space do not contain the constant vector on physical elements [25, 27, 26]. Optimal approximation and superconvergence properties in some MFE methods can be obtained under a grid restrictions to h^2-perturbed parallelograms or parallelepipeds [17, 34, 20]. Highly distorted quadrilaterals and hexahedra are treated using enriched Raviart-Thomas spaces in [6, 18] or composite-element techniques in [23, 27]. All of these methods require solving saddle point problems in their standard forms.

In [32], we developed an accurate MFMFE method on highly distorted hexahedra using a non-symmetric quadrature rule and an enhanced $BDDF_1$ space. The space does not contain constant velocity vectors and therefore does not have optimal approximation properties. However, we found that on element faces the space does have approximation properties and we employed techniques from the analysis of mimetic finite difference (MFD) methods [10, 24] to establish first order convergence for the pressure at the cell centers and the normal velocity on the element faces. The analysis applies to hexahedra with non-planar faces. In this paper, we develop an efficient local post-processing technique for the MFMFE method on hexahedra based on the enriched space introduced in [18]. This results in first order accurate velocities in the interior of the elements. Such velocities are suitable for transport of chemical species in subsurface simulations and saturation equation in multiphase flow simulations [28, 30]. In fact, the postprocessing works for any method that gives accurate face velocities on hexahedra, more precisely with velocity satisfying condition (2.26) in Theorem 2.2. For example, the MPFA O-method in physical space [1] is shown to be closely related and in some cases equivalent to the MFMFE method [22, 3], so the postprocessing also applies to the MPFA O-method.

This paper is divided into five additional sections. In Section 2, we discuss the multipoint flux method for the non-symmetric formulation, reduction to a cell centered pressure system, and a brief summary of convergence results. In Section 3, an enhancement of the $\mathcal{FGM}$ mixed finite element for general hexahedra formulated by Falk, Gatto, and Monk [18] is introduced. Convergence results are established for these enhanced spaces. These new spaces combined with an appropriate quadrature rule allow one to obtain a cell-centered pressure scheme with accurate face fluxes that can then be postprocessed to accurate velocities in the interior of the elements. The local postprocessing of velocities is formulated and analyzed in Section 4. Section 5 provides computational examples that verify the theoretical accuracy of the postprocessing. In Section 6 we summarize the results of the paper. Three appendices that provide bases for the velocities and the matrix representation of the local postprocessing have been added for completeness.

2. Multipoint flux mixed finite element method

Single phase incompressible flow in porous media is governed by coupled Darcy's law and continuity equation:

$$(2.1) \qquad \mathbf{u} = -K\nabla p,$$

$$(2.2) \qquad \nabla \cdot \mathbf{u} = f,$$

where p is the pressure, $\mathbf{u}$ is the Darcy velocity, K represents the rock permeability divided by fluid kinematic viscosity, and f is the source term. We consider the system (2.1)–(2.2) in a domain $\Omega \subset \mathbb{R}^3$ with Lipschitz continuous boundary. For simplicity we assume homogeneous Dirichlet boundary conditions

$$p = 0 \quad \text{on } \partial\Omega,$$

although more general boundary conditions can also be treated. We assume that K is a symmetric and uniformly positive definite tensor with $L^\infty(\Omega)$ components satisfying, for some $0 < k_0 \le k_1 < \infty$,

$$(2.3) \qquad k_0 \xi^T \xi \le \xi^T K(\mathbf{x})\xi \le k_1 \xi^T \xi, \quad \forall \mathbf{x} \in \Omega, \text{ and } \forall \xi \in \mathbb{R}^3.$$

Let $\mathcal{T}_h$ be a conforming, shape-regular, quasi-uniform partition of Ω [12], consisting of hexahedra with possibly non-planar faces. Let $W_{\mathcal{T}_h}^{k,\infty}$ consist of functions ϕ such that $\phi|_E \in W^{k,\infty}(E)$ for all $E \in \mathcal{T}_h$. Here k is a multi-index with integer components and $W^{k,\infty}(E)$ denotes the Sobolev space of functions whose derivatives of order k belong to $L^\infty(E)$. Let $\|\cdot\|_k$ be the norm in the Hilbert space $H^k(\Omega)$ with functions whose derivatives of order k belong to $L^2(\Omega)$. The norm in $L^2(\Omega)$ is denoted by $\|\cdot\|$. Let $X \lesssim (\gtrsim) Y$ denote that there exists a constant C, independent of the mesh size h, such that $X \le (\ge) CY$. The notation $X \approx Y$ means that both $X \lesssim Y$ and $X \gtrsim Y$ hold.

We assume that for any $E \in \mathcal{T}_h$ there exists a trilinear bijection mapping $F_E : \hat{E} \to E$, where $\hat{E}$ is the reference cube. Denote the Jacobian matrix by DF_E and let $J_E = |\det(DF_E)|$. Denote the inverse mapping by F_E^{-1}, its Jacobian matrix by DF_E^{-1}, and let $J_{F_E^{-1}} = |\det(DF_E^{-1})|$. We have that

$$DF_E^{-1}(\mathbf{x}) = (DF_E)^{-1}(\hat{\mathbf{x}}), \quad J_{F_E^{-1}}(\mathbf{x}) = \frac{1}{J_E(\hat{\mathbf{x}})}.$$

Using the above mapping definitions and the classical formula, for scalar $\phi(\mathbf{x}) = \hat{\phi}(\hat{\mathbf{x}})$, $\nabla\phi = (DF_E^{-1})^T \hat{\nabla}\hat{\phi}$, it is easy to see that, for any face $e_i \subset E$, the unit normal vector and Jacboian matrix are

$$(2.4) \qquad \mathbf{n}_i = \frac{1}{J_{e_i}} J_E (DF_E^{-1})^T \hat{\mathbf{n}}_i, \quad J_{e_i} = |J_E (DF_E^{-1})^T \hat{\mathbf{n}}_i|_{\mathbb{R}^3},$$

where $\hat{\mathbf{n}}_i$ is the unit normal vector with respect to the reference face $\hat{e}_i$, and $|\cdot|_{\mathbb{R}^3}$ is the Euclidean norm in $\mathbb{R}^3$. Also, the shape regularity and quasi-uniformity of the grids imply that, for all $E \in \mathcal{T}_h$,

$$(2.5) \qquad \begin{aligned} &\|DF_E\|_{0,\infty,\hat{E}} \lesssim h, \qquad \|DF_E^{-1}\|_{0,\infty,E} \lesssim h^{-1}, \\ &\|J_E\|_{0,\infty,\hat{E}} \approx h^3, \qquad \|J_{F_E^{-1}}\|_{0,\infty,E} \approx h^{-3}, \qquad \|J_e\|_{0,\infty,e} \approx h^2. \end{aligned}$$

The velocity and pressure finite element spaces on any physical element E are defined, respectively, via the Piola transformation

$$(2.6) \qquad \mathbf{v} \leftrightarrow \hat{\mathbf{v}} : \mathbf{v} = \frac{1}{J_E} DF_E \hat{\mathbf{v}} \circ F_E^{-1},$$

and the scalar transformation

$$w \leftrightarrow \hat{w} : w = \hat{w} \circ F_E^{-1}.$$

The Piola transformation preserves the normal components of the vectors:

$$(2.7) \qquad \mathbf{v} \cdot \mathbf{n}_e = \frac{1}{J_e} \hat{\mathbf{v}} \cdot \hat{\mathbf{n}}_{\hat{e}} \circ F_E^{-1}.$$

The finite element spaces $\mathbf{V}_h$ and W_h on $\mathcal{T}_h$ are given by

$$(2.8) \qquad \begin{aligned} \mathbf{V}_h &= \left\{ \mathbf{v} \in H(\mathbf{div}; \Omega) : \quad \mathbf{v}|_E \leftrightarrow \hat{\mathbf{v}}, \ \hat{\mathbf{v}} \in \hat{\mathbf{V}}(\hat{E}), \quad \forall E \in \mathcal{T}_h \right\}, \\ W_h &= \left\{ w \in L^2(\Omega) : \quad w|_E \leftrightarrow \hat{w}, \ \hat{w} \in \hat{W}(\hat{E}), \quad \forall E \in \mathcal{T}_h \right\}, \end{aligned}$$

where $\hat{\mathbf{V}}(\hat{E})$ and $\hat{W}(\hat{E})$ are finite element spaces on the reference element $\hat{E}$.

The velocity space $\hat{\mathbf{V}}(\hat{E})$ on the reference cube is defined by enhancing the $\mathcal{BDDF}_1$ spaces [20]:

$$(2.9)$$
$$\hat{\mathbf{V}}(\hat{E}) = \mathcal{BDDF}_1(\hat{E}) + \frac{R_1}{2}\mathrm{curl}(\hat{x}\hat{y}^2, 0, 0)^T + \frac{R_2}{2}\mathrm{curl}(0, \hat{y}\hat{z}^2, 0)^T + \frac{R_3}{2}\mathrm{curl}(0, 0, \hat{x}^2\hat{z})^T$$
$$+ S_1\mathrm{curl}(\hat{x}\hat{y}^2\hat{z}, 0, 0)^T + S_2(0, \hat{x}\hat{y}\hat{z}^2, 0)^T + S_3(0, 0, \hat{x}^2\hat{y}\hat{z})^T,$$

where the $\mathcal{BDDF}_1(\hat{E})$ space [7] is defined as

$$(2.10)$$
$$\mathcal{BDDF}_1(\hat{E}) = (P_1(\hat{E}))^3 + E_1\mathrm{curl}(\hat{x}\hat{y}\hat{z}, 0, 0)^T + E_2\mathrm{curl}(0, \hat{x}\hat{y}\hat{z}, 0)^T + E_3\mathrm{curl}(0, 0, \hat{x}\hat{y}\hat{z})^T$$
$$- G_1\mathrm{curl}(\hat{x}\hat{y}\hat{z}, \hat{x}^2\hat{z}, 0)^T - G_2\mathrm{curl}(0, \hat{x}\hat{y}\hat{z}, \hat{x}\hat{y}^2)^T - G_3\mathrm{curl}(\hat{y}\hat{z}^2, 0, \hat{x}\hat{y}\hat{z})^T.$$

The pressure space on the reference cube is defined as

$$\hat{W}(\hat{E}) = P_0(\hat{E}).$$

In above equations, R_i, S_i, E_i, G_i $(i = 1, \ldots, 3)$ are real constants, P_k denotes the space of polynomials of degree at most k, and $(\hat{x}, \ \hat{y}, \ \hat{z})^T$ denotes a point in the reference element. The enhancement of the $\mathcal{BDDF}_1$ space is needed to obtain a space with four degrees of freedom (DOF) per face, rather than three in the original formulation. This allows to associate a degree of freedom with each vertex of the face, which is needed in the reduction to a cell-centered pressure stencil as described later in this section.

The multipoint flux mixed finite element (MFMFE) method [32, 31] is defined as follows: find $\mathbf{u}_h \in \mathbf{V}_h$ and $p_h \in W_h$ such that

$$(2.11) \qquad (K^{-1}\mathbf{u}_h, \mathbf{v})_Q - (p_h, \nabla \cdot \mathbf{v}) = 0, \qquad \forall \mathbf{v} \in \mathbf{V}_h,$$
$$(2.12) \qquad (\nabla \cdot \mathbf{u}_h, w) = (f, w), \qquad \forall w \in W_h.$$

A key ingredient in the MFMFE method is the numerical quadrature rule for $(K^{-1}\cdot, \cdot)_Q$. The integration for the velocity mass matrix on any element E is performed by mapping to the reference element $\hat{E}$ and applying a quadrature rule defined on $\hat{E}$. Using (2.8) and (2.6), for all $\mathbf{q}, \mathbf{v} \in \mathbf{V}_h$, we have

$$(K^{-1}\mathbf{q}, \mathbf{v})_E = \left(\frac{1}{J_E} DF_E^T K^{-1}(F_E(\hat{\mathbf{x}})) DF_E \hat{\mathbf{q}}, \hat{\mathbf{v}} \right)_{\hat{E}} \equiv (\mathcal{M}_E \hat{\mathbf{q}}, \hat{\mathbf{v}})_{\hat{E}},$$

where

$$(2.13) \qquad \mathcal{M}_E(\hat{\mathbf{x}}) = \frac{1}{J_E(\hat{\mathbf{x}})} DF_E^T(\hat{\mathbf{x}}) K^{-1}(F_E(\hat{\mathbf{x}})) DF_E(\hat{\mathbf{x}}).$$

Define a constant matrix $\overline{K}_E$ such that $\overline{K}_E^{ij}$ is the mean value of K^{ij} on E, where $\overline{K}_E^{ij}$ and K^{ij} denote the elements on the i-th row and j-th column of matrix $\overline{K}_E$ and K respectively. Let $\hat{\mathbf{r}}_{c,\hat{E}}$ denote the center of mass of $\hat{E}$. Replacing DF_E^T and K by the constant matrices $DF_E^T(\hat{\mathbf{r}}_{c,\hat{E}})$ and $\overline{K}_E$ respectively, we define

$$(2.14) \qquad \widetilde{\mathcal{M}}_E(\hat{\mathbf{x}}) = \frac{1}{J_E(\hat{\mathbf{x}})} DF_E^T(\hat{\mathbf{r}}_{c,\hat{E}}) \overline{K}_E^{-1} DF_E(\hat{\mathbf{x}}).$$

In addition, we use $(\cdot,\cdot)_{\hat{Q},\hat{E}}$ to denote the trapezoidal rule on $\hat{E}$:

$$(2.15) \qquad (\hat{\mathbf{q}}, \hat{\mathbf{v}})_{\hat{Q},\hat{E}} \equiv \frac{|\hat{E}|}{8} \sum_{i=1}^{8} \hat{\mathbf{q}}(\hat{\mathbf{r}}_i) \cdot \hat{\mathbf{v}}(\hat{\mathbf{r}}_i),$$

where $\hat{\mathbf{r}}_i$ are the vertices of element $\hat{E}$.

The quadrature rule on an element E is defined as

$$(2.16) \qquad (K^{-1}\mathbf{q}, \mathbf{v})_{Q,E} \equiv (\widetilde{\mathcal{M}}_E \hat{\mathbf{q}}, \hat{\mathbf{v}})_{\hat{Q},\hat{E}} = \frac{|\hat{E}|}{8} \sum_{i=1}^{8} \widetilde{\mathcal{M}}_E(\hat{\mathbf{r}}_i) \hat{\mathbf{q}}(\hat{\mathbf{r}}_i) \cdot \hat{\mathbf{v}}(\hat{\mathbf{r}}_i).$$

Mapping back to the physical element E, we have the quadrature rule on E:

$$(2.17) \qquad (K^{-1}\mathbf{q}, \mathbf{v})_{Q,E} = \frac{1}{8} \sum_{i=1}^{8} J_E(\hat{\mathbf{r}}_i)(DF_E^{-1})^T(\mathbf{r}_i) DF_E^T(\hat{\mathbf{r}}_{c,\hat{E}}) \overline{K}_E^{-1} \mathbf{q}(\mathbf{r}_i) \cdot \mathbf{v}(\mathbf{r}_i).$$

Note that the trapezoidal rule for the modified integrand induces a non-symmetric quadrature rule unless the Jacobian matrix DF_E is constant. This is related to a non-symmetric inner product used in mimetic finite difference methods [19, 24]. A similar quadrature rule on quadrilateral elements was introduced in [22], where the mean value of K^{-1} was used. Our analysis in [32] applies also in that case with an extra term involving the difference between $\overline{K}_E^{-1}$ and $\overline{K_E^{-1}}$, which is of order $\mathcal{O}(h)$.

The global quadrature rule on Ω is defined as

$$(K^{-1}\mathbf{q}, \mathbf{v})_Q \equiv \sum_{E \in \mathcal{T}_h} (K^{-1}\mathbf{q}, \mathbf{v})_{Q,E}.$$

Remark 2.1. *The symmetric version of the method based on $\mathcal{M}_E$ from (2.13) has been shown to work well for simplicial grids and smooth or h^2-perturbed quadrilateral and hexahedral grids [34, 20, 33]. Furthermore, it is always coercive, while the non-symmetric method has a coercivity condition (2.19) that may not be satisfied in some extreme cases. However, the performance of the symmetric method deteriorates on rough grids and we do not consider it in this paper. Instead, we focus on the non-symmetric method, which provides first order accurate fluxes on element faces on general hexahedra. This is due to the fact that the non-symmetric quadrature rule based on (2.14) satisfies some critical properties on the physical elements that are key ingredients in the error analysis. The reader is referred to [32] for details.*

2.1. Reduction to a cell-centered pressure system. The choice of trapezoidal quadrature rule implies that on each element, the velocity DOF associated with a vertex become decoupled from the rest of the DOF. As a result, the assembled velocity mass matrix in (2.11) has a block-diagonal structure with one block per grid vertex. The dimension of each block equals the number of velocity DOF associated with the vertex. In particular,

$$(2.18) \qquad (K^{-1}\mathbf{q}, \mathbf{v})_Q = \sum_{E \in \mathcal{T}_h} (K^{-1}\mathbf{q}, \mathbf{v})_{Q,E} \equiv \sum_{c \in \mathcal{C}_h} \mathbf{v}_c^T \mathbf{M}_c \mathbf{q}_c,$$
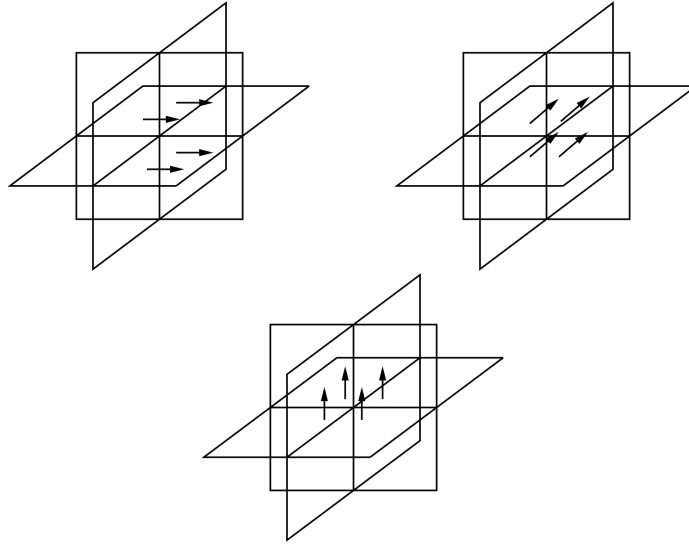
FIGURE 2. Interactions of the velocity degrees of freedom in the MFMFE method

where $\mathcal{C}_h$ denotes the set of corner or vertex points in $\mathcal{T}_h$, $\mathbf{v}_c := \{(\mathbf{v} \cdot \mathbf{n}_e)(\mathbf{x}_c)\}_{e=1}^{n_c}$ with a similar definition for $\mathbf{q}_c$, $\mathbf{x}_c$ is the coordinate vector of point c, n_c is the number of faces that share the vertex point c, and $\mathbf{M}_c$ is an $n_c \times n_c$ matrix, see [32] for further details. For example, $n_c = 12$ for logically rectangular hexahedral grids, see Figure 2. Inverting each local block in the mass matrix in (2.11) allows for expressing the velocity DOF associated with a vertex in terms of the pressures at the centers of the elements that share the vertex (there are eight such elements in Figure 2). Substituting these expressions into the mass conservation equation (2.12) leads to a cell-centered system for the pressures. The stencil is 27 points on logically rectangular hexahedral grids. The local linear systems and the resulting global pressure system are positive definite and therefore invertible under a mild restriction on the shape regularity of the grids and/or the anisotropy of the permeability, see (2.19) below.

2.2. Convergence of the MFMFE method.
For the analysis of the non-symmetric MFMFE method, we require some properties of the bilinear form $(K^{-1}\cdot, \cdot)_Q$ defined on the space $\mathbf{V}_h$.

Lemma 2.1 ([32]). *Assume that $\mathbf{M}_c$ is uniformly positive definite for all $c \in \mathcal{C}_h$:*

$$(2.19) \qquad h^3 \boldsymbol{\xi}^T \boldsymbol{\xi} \lesssim \boldsymbol{\xi}^T \mathbf{M}_c \boldsymbol{\xi}, \quad \forall \boldsymbol{\xi} \in \mathbb{R}^{n_c}.$$

Then the bilinear form $(K^{-1}\cdot, \cdot)_Q$ is coercive in $\mathbf{V}_h$ and induces a norm in $\mathbf{V}_h$ equivalent to the L^2-norm:

$$(2.20) \qquad (K^{-1}\mathbf{v}, \mathbf{v})_Q \approx \|\mathbf{v}\|^2, \quad \forall \mathbf{v} \in \mathbf{V}_h.$$

If in addition

$$(2.21) \qquad \boldsymbol{\xi}^T \mathbf{M}_c^T \mathbf{M}_c \boldsymbol{\xi} \lesssim h^6 \boldsymbol{\xi}^T \boldsymbol{\xi}, \quad \forall \boldsymbol{\xi} \in \mathbb{R}^{n_c},$$

then the following Cauchy-Schwarz type inequality holds:

$$(2.22) \qquad (K^{-1}\mathbf{q}, \mathbf{v})_Q \lesssim \|\mathbf{q}\| \|\mathbf{v}\| \quad \forall \mathbf{q}, \mathbf{v} \in \mathbf{V}_h,$$

Conditions (2.19) and (2.21) impose mild restrictions on the element geometry and the anisotropy of the permeability tensor K, see [22, 24].

Recall the canonical interpolation operator in the space $\mathbf{V}_h$. The reference interpolant $\hat{\Pi} : (H^1(\hat{E}))^3 \to \hat{\mathbf{V}}(\hat{E})$ is defined by

$$(2.23) \qquad \forall \hat{e} \subset \partial \hat{E}, \quad \langle (\hat{\Pi}\hat{\mathbf{q}} - \hat{\mathbf{q}}) \cdot \hat{\mathbf{n}}_{\hat{e}}, \hat{q}_1 \rangle_{\hat{e}} = 0, \quad \forall \hat{q}_1 \in Q_1(\hat{e}),$$

where Q_1 is the space of bilinear functions. The global operator $\Pi : \mathbf{V} \cap (H^1(\Omega))^3 \to \mathbf{V}_h$ on each element E is defined by the Piola transformation:

$$(2.24) \qquad \qquad \Pi\mathbf{q} \leftrightarrow \widehat{\Pi\mathbf{q}}, \quad \widehat{\Pi\mathbf{q}} = \hat{\Pi}\hat{\mathbf{q}}.$$

Note that (2.7) and (2.23) imply that $\Pi\mathbf{q} \cdot \mathbf{n}$ is continuous across element interfaces, which gives $\Pi\mathbf{q} \in \mathbf{V}_h$.

Theorem 2.1 ([32]). *Let $K \in W^{1,\infty}_{\mathcal{T}_h}(\Omega)$ and $K^{-1} \in W^{0,\infty}(\Omega)$. If (2.19) and (2.21) hold, then the pressure p_h and the velocity $\mathbf{u}_h$ of the non-symmetric MFMFE method (2.11)—(2.12) satisfy*

$$(2.25) \qquad \qquad \|p - p_h\| + \|\Pi\mathbf{u} - \mathbf{u}_h\| \lesssim h(|\mathbf{u}|_1 + \|p\|_2).$$

Theorem 2.2 ([32]). *Let $K \in W^{1,\infty}_{\mathcal{T}_h}(\Omega)$ and $K^{-1} \in W^{0,\infty}_{\mathcal{T}_h}(\Omega)$. If (2.19) and (2.21) hold, then the velocity $\mathbf{u}_h$ of the non-symmetric MFMFE method (2.11)—(2.12) satisfies*

$$(2.26) \qquad \left(\sum_{E \in \mathcal{T}_h} \|(\mathbf{u} - \mathbf{u}_h) \cdot \mathbf{n}_e\|^2_{\partial E} \right)^{1/2} \lesssim h^{1/2}(\|\mathbf{u}\|_1 + \|p\|_2).$$

We remark that the shape regularity assumption on the mesh implies that $|E|/|\partial E| \approx h$; hence the above theorem gives $O(h)$ convergence for the face fluxes.

3. The enhanced $\mathcal{FGM}$ mixed finite element method

The $\mathcal{FGM}$ mixed finite element space on general hexahedra [18] was constructed to be $H(\mathbf{div})$-conforming and contain the space of constants on any physical element E. This results in an $O(h)$ convergent mixed finite element method. This is the mixed velocity space with the fewest known DOF with such property. Here we introduce an enhanced $\mathcal{FGM}$, which will be used in our postprocessing procedure.

3.1. The enhanced $\mathcal{FGM}$ space.
The $\mathcal{FGM}$ space $\hat{\mathbf{S}}_0$ [18] consists of all vectors $\hat{\mathbf{u}} = (\hat{u}_1, \hat{u}_2, \hat{u}_3)^T$ on $\hat{E}$ of the form:

(3.1)
$$\hat{u}_1 = A_1 + B_1\hat{x} + C_1\hat{y} + D_1\hat{z} - (E_2 + G_2)\hat{x}\hat{y} + (E_3 - G_3)\hat{x}\hat{z} + G_1\hat{x}^2 + H_3\hat{x}^2\hat{y} - H_2\hat{x}^2\hat{z},$$
$$\hat{u}_2 = A_2 + B_2\hat{x} + C_2\hat{y} + D_2\hat{z} + (E_1 - G_1)\hat{y}\hat{x} - (E_3 + G_3)\hat{y}\hat{z} + G_2\hat{y}^2 - H_3\hat{x}\hat{y}^2 + H_1\hat{y}^2\hat{z},$$
$$\hat{u}_3 = A_3 + B_3\hat{x} + C_3\hat{y} + D_3\hat{z} - (E_1 + G_1)\hat{z}\hat{x} + (E_2 - G_2)\hat{z}\hat{y} + G_3\hat{z}^2 + H_2\hat{x}\hat{z}^2 - H_1\hat{y}\hat{z}^2,$$

where $A_i, B_i, C_i, D_i, E_i, G_i, H_i$ are constants. For $\hat{\mathbf{u}} \in \hat{\mathbf{S}}_0$, the 21 DOF are given by

- $\langle \hat{\mathbf{u}} \cdot \hat{\mathbf{n}}, \hat{q} \rangle_{\hat{e}}, \quad \forall \hat{q} \in P_1(\hat{e}), \ \forall \hat{e} \subset \partial \hat{E},$
- $(\hat{\mathbf{u}}, \hat{\mathbf{r}})_{\hat{E}}, \quad \forall \hat{\mathbf{r}} \in \hat{\mathcal{R}}$, where $\hat{\mathcal{R}}$ denotes the span of the vectors

$$\hat{\mathbf{r}}_1 := (0, 1/2 - \hat{z}, \hat{y} - 1/2)^T, \ \hat{\mathbf{r}}_2 := (1/2 - \hat{z}, 0, \hat{x} - 1/2)^T, \ \hat{\mathbf{r}}_3 := (1/2 - \hat{y}, \hat{x} - 1/2, 0)^T.$$

The space $\hat{\mathbf{S}}_0$ can also be written as

(3.2)
$$\hat{\mathbf{S}}_0 = \mathcal{BDDF}_1(\hat{E}) + H_1(0, \hat{y}^2\hat{z}, -\hat{y}\hat{z}^2)^T + H_2(-\hat{x}^2\hat{z}, 0, \hat{x}\hat{z}^2)^T + H_3(\hat{x}^2\hat{y}, -\hat{x}\hat{y}^2, 0)^T$$

$$= \mathcal{BDDF}_1(\hat{E}) + \frac{H_1}{2}\text{curl}(\hat{y}^2\hat{z}^2, 0, 0)^T + \frac{H_2}{2}\text{curl}(0, \hat{x}^2\hat{z}^2, 0)^T + \frac{H_3}{2}\text{curl}(0, 0, \hat{x}^2\hat{y}^2)^T,$$

We are now ready to define the enhanced $\mathcal{FGM}$ space as

(3.3)
$$\hat{\mathbf{V}}^*(\hat{E}) := \hat{\mathbf{S}}_0 \cup \hat{\mathbf{V}}(\hat{E}),$$

where $\hat{\mathbf{V}}(\hat{E})$ is the enhanced $\mathcal{BDDF}_1$ space defined in (2.9). For $\hat{\mathbf{u}} \in \hat{\mathbf{V}}^*(\hat{E})$, there are 27 DOF given by

- $\langle \hat{\mathbf{u}} \cdot \hat{\mathbf{n}}, \hat{q} \rangle_{\hat{e}}, \quad \forall \hat{q} \in Q_1(\hat{e}), \ \forall \hat{e} \subset \partial\hat{E},$
- $(\hat{\mathbf{u}}, \hat{\mathbf{r}})_{\hat{E}}, \quad \forall \hat{\mathbf{r}} \in \hat{\mathcal{R}}.$

The following lemma establishes the unisolvence of the $\hat{\mathbf{V}}^*(\hat{E})$. The proof is similar to the unisolvence of $\hat{\mathbf{S}}_0$ in [18] and is given here for completeness.

Lemma 3.1. *Any $\hat{\mathbf{v}} \in \hat{\mathbf{V}}^*(\hat{E})$ is uniquely determined by the DOF in $\hat{\mathbf{V}}^*(\hat{E})$.*

Proof. It is enough to show $\hat{\mathbf{v}} = 0$ if the DOF are all zero. By definition, we can write $\hat{\mathbf{v}} := (\hat{v}_1, \hat{v}_2, \hat{v}_3) \in \hat{\mathbf{V}}^*(\hat{E})$ as

(3.4)
$$\hat{v}_1 = \hat{u}_1 - R_2\hat{y}\hat{z} + S_3\hat{x}^2\hat{z} - 2S_2\hat{x}\hat{y}\hat{z},$$
$$\hat{v}_2 = \hat{u}_2 - R_3\hat{x}\hat{z} + S_1\hat{x}\hat{y}^2 - 2S_3\hat{x}\hat{y}\hat{z},$$
$$\hat{v}_3 = \hat{u}_3 - R_1\hat{x}\hat{y} + S_2\hat{y}\hat{z}^2 - 2S_1\hat{x}\hat{y}\hat{z},$$

where $\hat{\mathbf{u}} := (\hat{u}_1, \hat{u}_2, \hat{u}_3)^T \in \hat{\mathbf{S}}_0$ given in (3.1). Note that the face DOF imply that $\hat{\mathbf{v}} \cdot \hat{\mathbf{n}} = 0$ on $\partial\hat{E}$. If $\hat{\mathbf{v}} \cdot \hat{\mathbf{n}} = 0$ on the face $\hat{x} = 0$, then $A_1 = C_1 = D_1 = R_2 = 0$. Similarly, using the DOF on faces $\hat{y} = 0$ and $\hat{z} = 0$, gives $A_2 = B_2 = D_2 = R_3 = 0$ and $A_3 = B_3 = C_3 = R_1 = 0$. The conditions $\hat{\mathbf{v}} \cdot \hat{\mathbf{n}} = 0$ on faces $\hat{x} = 1$, $\hat{y} = 1$, and $\hat{z} = 1$, give the following:

$$B_1 + G_1 = 0, \quad -E_2 - G_2 + H_3 = 0, \quad E_3 - G_3 - H_2 + S_3 = 0, \quad S_2 = 0$$
$$C_2 + G_2 = 0, \quad E_1 - G_1 - H_3 + S_1 = 0, \quad -E_3 - G_3 + H_1 = 0, \quad S_3 = 0,$$
$$D_3 + G_3 = 0, \quad -E_1 - G_1 + H_2 = 0, \quad E_2 - G_2 - H_1 + S_2 = 0, \quad S_1 = 0.$$

Solving the above equations in terms of H_1, H_2, and H_3 gives

$$B_1 = (H_3 - H_2)/2, \quad E_1 = (H_2 + H_3)/2, \quad G_1 = (H_2 - H_3)/2,$$
$$C_2 = (H_1 - H_3)/2, \quad E_2 = (H_1 + H_3)/2, \quad G_2 = (H_3 - H_1)/2,$$
$$D_3 = (H_2 - H_1)/2, \quad E_3 = (H_1 + H_2)/2, \quad G_3 = (H_1 - H_2)/2.$$

Hence, if the 24 DOF of $\hat{\mathbf{v}}$ on the faces are zero, $\hat{\mathbf{v}}$ has the form

(3.5)
$$\hat{v}_1 = \hat{x}(1 - \hat{x})\left[H_2(\hat{z} - 1/2) - H_3(\hat{y} - 1/2)\right],$$
$$\hat{v}_2 = \hat{y}(1 - \hat{y})\left[H_3(\hat{x} - 1/2) - H_1(\hat{z} - 1/2)\right],$$
$$\hat{v}_3 = \hat{z}(1 - \hat{z})\left[H_1(\hat{y} - 1/2) - H_2(\hat{x} - 1/2)\right].$$

If the remaining three DOF are zero, it is easy to verify that $H_1 = H_2 = H_3 = 0$. $\square$

The global spaces $\mathbf{V}_h^*$ and W_h^* are defined similarly to (2.8). The operator $\hat{\Pi}^* : (H^1(\hat{E}))^3 \to \hat{\mathbf{V}}^*(\hat{E})$ is defined by

(3.6)
$$\langle (\hat{\Pi}^*\hat{\mathbf{v}} - \hat{\mathbf{v}}) \cdot \hat{\mathbf{n}}_{\hat{e}}, \hat{q}_1 \rangle_{\hat{e}} = 0, \quad \forall \hat{e} \subset \partial\hat{E}, \quad \hat{q}_1 \in Q_1(\hat{e})$$
$$(\hat{\Pi}^*\hat{\mathbf{v}} - \hat{\mathbf{v}}, \hat{\mathbf{r}})_{\hat{E}} = 0, \quad \forall \hat{\mathbf{r}} \in \hat{\mathcal{R}}.$$

The global operator $\Pi^* : \mathbf{V}^* \cap (H^1(\Omega))^3 \to \mathbf{V}_h^*$ on each element E is defined by the Piola transformation:

$$(3.7) \qquad \Pi^* \mathbf{v} \leftrightarrow \widehat{\Pi^* \mathbf{v}}, \quad \widehat{\Pi^* \mathbf{v}} = \hat{\Pi}^* \hat{\mathbf{v}}.$$

Lemma 3.2. *For* $\mathbf{q} \in (H^1(\Omega))^3$,

$$(3.8) \qquad \|\mathbf{q} - \Pi^* \mathbf{q}\|_E \lesssim h|\mathbf{q}|_{1,E}, \quad \forall E \in \mathcal{T}_h.$$

Proof. The proof is similar to the one in [18], using the fact that Π^* preserves the constant vectors. □

Lemma 3.3. *For* $\mathbf{q} \in (H^1(E))^3$,

$$(3.9) \qquad \|\Pi^* \mathbf{q}\|_E \lesssim \|\mathbf{q}\|_E + h|\mathbf{q}|_{1,E}.$$

$$(3.10) \qquad \|\nabla \cdot \Pi^* \mathbf{q}\|_E \lesssim \|\nabla \cdot \mathbf{q}\|_E.$$

Proof. The proof is based on a scaling argument for the Piola transformation. We refer to [32] for details. □

3.2. Convergence of the enhanced $\mathcal{FGM}$ mixed finite element method. The enhanced $\mathcal{FGM}$ mixed finite element is defined as follows: find $\mathbf{u}_h^* \in \mathbf{V}_h^*$ and $p_h^* \in W_h$ such that

$$(3.11) \qquad (K^{-1} \mathbf{u}_h^*, \mathbf{v}) - (p_h^*, \nabla \cdot \mathbf{v}) = 0, \qquad \forall \mathbf{v} \in \mathbf{V}_h^*,$$

$$(3.12) \qquad (\nabla \cdot \mathbf{u}_h^*, w) = (f, w), \quad \forall w \in W_h.$$

Following the classical mixed finite element theory [9], we have the following result.

Theorem 3.1. *There exists a unique solution* $\{\mathbf{u}_h^*, p_h^*\}$ *of the enhanced* $\mathcal{FGM}$ *method* (3.11)–(3.12) *that satisfies*

$$(3.13) \qquad \|\mathbf{u} - \mathbf{u}_h^*\| \lesssim h|\mathbf{u}|_1,$$

$$(3.14) \qquad \|p - p_h^*\| \lesssim h(|\mathbf{u}|_1 + \|p\|_1).$$

Remark 3.1. *Since* Π^* *has no interpolation estimate under the divergence norm,* $\mathbf{u}_h^*$ *has no divergence error estimate as well.*

The rest of this section is devoted to establishing the convergence of the velocity on the element faces. We start with several auxiliary lemmas needed in the analysis.

Lemma 3.4 ([32]). *For any element* $E \in \mathcal{T}_h$,

$$(3.15) \qquad \|\hat{\mathbf{q}}\|_{\hat{E}} \approx h^{1/2} \|\mathbf{q}\|_E, \quad \forall \mathbf{q} \in (L^2(E))^3,$$

$$(3.16) \qquad |\hat{\mathbf{q}}|_{1,\hat{E}} \lesssim (h^{1/2} \|\mathbf{q}\|_E + h^{3/2} |\mathbf{q}|_{1,E}), \quad \forall \mathbf{q} \in (H^1(E))^3.$$

Lemma 3.5. *The following trace inequality holds*

$$(3.17) \qquad \|\mathbf{v} \cdot \mathbf{n}_e\|_e \lesssim h^{-1/2} \|\mathbf{v}\|_E, \quad \forall \mathbf{v} \in \mathbf{V}_h^*, \ \forall e \in \partial E.$$

Proof. Using the trace inequality [4, 5] on the reference element $\hat{E}$, we have

$$\|\hat{\mathbf{v}} \cdot \hat{\mathbf{n}}_{\hat{e}}\|_{\hat{e}} \lesssim \|\hat{\mathbf{v}}\|_{\hat{E}} + |\hat{\mathbf{v}}|_{1,\hat{E}} \lesssim \|\hat{\mathbf{v}}\|_{\hat{E}},$$

where we also used the norm equivalence on reference element in the second inequality. The result follows from (3.15), (2.7), and (2.5). □

Lemma 3.6. *For any constant vector* $\mathbf{q}_0$ *on* E,

$$(3.18) \qquad \forall e \subset \partial E, \quad \Pi^* \mathbf{q}_0 \cdot \mathbf{n}_e = \mathbf{q}_0 \cdot \mathbf{n}_e.$$

Proof. In [32], Lemma 3.6 and Remark 3.2 show that the Piola image of a constant vector on a physical element has a linear normal component in the reference element. Thus $\hat{\Pi}^*\hat{\mathbf{q}}_0 \cdot \hat{\mathbf{n}}_e = \hat{\mathbf{q}}_0 \cdot \hat{\mathbf{n}}_e$ since the enhanced $\mathcal{FGM}$ space has a bilinear normal component in the reference element. $\square$

Lemma 3.7. *For* $\mathbf{u} \in (H^1(E))^3$,

$$(3.19) \qquad \|(\mathbf{u} - \Pi^*\mathbf{u}) \cdot \mathbf{n}_e\|_e \lesssim h^{1/2}|\mathbf{u}|_{1,E}, \quad \forall e \in \partial E.$$

Proof. Let $\mathbf{q}$ be any constant vector on E. Lemma 3.6 implies that

$$(3.20) \qquad \begin{aligned} \|(\mathbf{u} - \Pi^*\mathbf{u}) \cdot \mathbf{n}_e\|_e &= \|(\mathbf{u} - \mathbf{q}_0) \cdot \mathbf{n}_e - (\Pi^*\mathbf{u} - \Pi^*\mathbf{q}_0) \cdot \mathbf{n}_e\|_e \\ &\leq \|(\mathbf{u} - \mathbf{q}_0) \cdot \mathbf{n}_e\|_e + \|\Pi^*(\mathbf{u} - \mathbf{q}_0) \cdot \mathbf{n}_e\|_e. \end{aligned}$$

Using the trace inequality for Lipschitz domains [4, 5],

$$(3.21) \qquad \forall e \subset \partial E, \quad \|\phi\|_e \lesssim h^{-1/2}\|\phi\|_E + h^{1/2}|\phi|_{1,E}, \quad \forall \phi \in H^1(E),$$

we have

$$(3.22) \qquad \|(\mathbf{u} - \mathbf{q}_0) \cdot \mathbf{n}_e\|_e \lesssim h^{-1/2}\|\mathbf{u} - \mathbf{q}_0\|_E + h^{1/2}|\mathbf{u} - \mathbf{q}_0|_{1,E}.$$

The trace inequality (3.17) gives that

$$(3.23) \quad \|\Pi^*(\mathbf{u}-\mathbf{q}_0)\cdot\mathbf{n}_e\|_e \lesssim h^{-1/2}\|\Pi^*(\mathbf{u}-\mathbf{q}_0)\|_E \lesssim h^{-1/2}\|\mathbf{u}-\mathbf{q}_0\|_E + h^{1/2}|\mathbf{u}-\mathbf{q}_0|_{1,E},$$

where we have also used (3.9) in the last inequality. Taking $\mathbf{q}_0$ to be the L^2-projection of $\mathbf{u}$ into the space of constant vectors on E in (3.20)–(3.23) yields (3.19) $\square$

Theorem 3.2. *The solution* $\{\mathbf{u}_h^*, p_h^*\}$ *of the enhanced* $\mathcal{FGM}$ *method* (3.11)–(3.12) *satisfies*

$$(3.24) \qquad \left(\sum_{E \in \mathcal{T}_h} \|(\mathbf{u} - \mathbf{u}_h^*) \cdot \mathbf{n}_e\|_{\partial E}^2\right)^{1/2} \lesssim h^{1/2}|\mathbf{u}|_1.$$

Proof. The triangle inequality gives

$$\begin{aligned} \|(\mathbf{u} - \mathbf{u}_h^*) \cdot \mathbf{n}_e\|_e &\leq \|(\mathbf{u} - \Pi^*\mathbf{u}) \cdot \mathbf{n}_e\|_e + \|(\Pi^*\mathbf{u} - \mathbf{u}_h^*) \cdot \mathbf{n}_e\|_e \\ &\lesssim h^{1/2}|\mathbf{u}|_{1,E} + h^{-1/2}\|\Pi^*\mathbf{u} - \mathbf{u}_h^*\|_E. \end{aligned}$$

where we have used (3.19) and (3.17) in the second inequality. The assertion of the theorem follows by combining the above inequality with (3.8) and (3.13). $\square$

4. Local velocity postprocessing

4.1. Definition of the method. The MFMFE method gives accurate face velocities, see Theorem 2.2. We use these face velocities as Neumann boundary conditions for the local auxiliary problem (2.1)–(2.2) in each element E:

$$(4.25) \qquad \tilde{\mathbf{u}} = -K\nabla\tilde{p}, \qquad \text{in } E,$$

$$(4.26) \qquad \nabla \cdot \tilde{\mathbf{u}} = f, \qquad \text{in } E,$$

$$(4.27) \qquad \tilde{\mathbf{u}} \cdot \mathbf{n}_e = \mathbf{u}_h \cdot \mathbf{n}_e, \quad \text{on } \partial E.$$

This problem satisfies the solvability condition

$$(4.28) \qquad \int_E f\,dx = \int_{\partial E} \tilde{\mathbf{u}} \cdot \mathbf{n}_e\,ds,$$

due to the local mass conservation property of the MFMFE method.

We use the enhanced $\mathcal{FGM}$ finite element method to solve this problem. Denote

$$(4.29) \qquad \mathbf{V}^*_{h,0}(E) := \{\mathbf{v} \in \mathbf{V}^*_h(E) \mid \mathbf{v} \cdot \mathbf{n}_E = 0 \text{ on } \partial E\}.$$

We seek $\mathcal{P}(\mathbf{u}_h) := \tilde{\mathbf{u}}_h \in \mathbf{V}^*_h$ with $\tilde{\mathbf{u}}_h \cdot \mathbf{n}_e = \mathbf{u}_h \cdot \mathbf{n}_e$ on ∂E and $\tilde{p}_h \in W_h(E)$ such that

$$(4.30) \qquad (K^{-1}\tilde{\mathbf{u}}_h, \mathbf{v})_E - (\tilde{p}_h, \nabla \cdot \mathbf{v})_E = 0, \qquad \forall \mathbf{v} \in \mathbf{V}^*_{h,0}(E),$$

$$(4.31) \qquad (\nabla \cdot \tilde{\mathbf{u}}_h, w)_E = (f, w)_E, \quad \forall w \in W_h(E).$$

The theory of the enhanced $\mathcal{FGM}$ method, see Theorem 3.1, implies that the above problem has a unique solution. Furthermore, by (4.27), (4.28), and (4.29), the above equations are equivalent to

$$(4.32) \qquad (K^{-1}\tilde{\mathbf{u}}_h, \mathbf{v})_E = 0, \quad \forall \mathbf{v} \in \mathbf{V}^*_{h,0}(E).$$

4.2. Convergence of the postprocessed velocity.

Lemma 4.1. *For any* $\mathbf{v} \in \mathbf{V}^*_h(E)$*, there exists* $\mathbf{v}_0 \in \mathbf{V}^*_{h,0}(E)$ *and* $\mathbf{v}_1 \in \mathbf{V}_h(E)$ *such that*

$$(4.33) \qquad \mathbf{v} = \mathbf{v}_0 + \mathbf{v}_1.$$

Proof. It is enough to show the existence on the reference element $\hat{E}$. Let $\hat{\mathbf{v}}_1 \in \hat{\mathbf{V}}(\hat{E})$ be the solution of

$$\langle \hat{\mathbf{v}}_1 \cdot \hat{\mathbf{n}}_{\hat{e}}, \hat{q} \rangle_{\hat{e}} = \langle \hat{\mathbf{v}} \cdot \hat{\mathbf{n}}_{\hat{e}}, \hat{q} \rangle_{\hat{e}}, \quad \forall \hat{q} \in Q_1(\hat{e}), \ \forall \hat{e} \in \partial \hat{E}.$$

The unisolvence of enhanced $\mathcal{BDDF}_1$ implies the existence and uniqueness of $\hat{\mathbf{v}}_1$. Next, let $\hat{\mathbf{v}}_0 \in \hat{\mathbf{V}}^*(\hat{E})$ be the solution of

$$\langle \hat{\mathbf{v}}_0 \cdot \hat{\mathbf{n}}_{\hat{e}}, \hat{q} \rangle_{\hat{e}} = 0, \qquad \forall \hat{q} \in Q_1(\hat{e}), \ \forall \hat{e} \in \partial \hat{E},$$

$$(\hat{\mathbf{v}}_0, \hat{\mathbf{r}})_{\hat{E}} = (\hat{\mathbf{v}} - \hat{\mathbf{v}}_1, \hat{\mathbf{r}})_{\hat{E}}, \qquad \forall \hat{\mathbf{r}} \in \hat{\mathbf{R}}.$$

Lemma 3.1 implies that such $\hat{\mathbf{v}}_0$ exists and is unique. By definition, it is easy to see that

$$\hat{\mathbf{v}} = \hat{\mathbf{v}}_0 + \hat{\mathbf{v}}_1, \quad \text{and} \quad \hat{\mathbf{v}}_0 \cdot \hat{\mathbf{n}}_{\hat{e}} = 0 \text{ on } \partial \hat{E}.$$

$\square$

Lemma 4.2. *The following trace inequality holds:*

$$(4.34) \qquad \|\mathbf{v} \cdot \mathbf{n}_e\|_{\partial E} \approx h^{-1/2}\|\mathbf{v}\|_E \quad \forall \mathbf{v} \in \mathbf{V}_h.$$

Proof. Since the DOF on $\mathbf{V}_h$ are all defined on the element faces, $\|\hat{\mathbf{v}} \cdot \hat{\mathbf{n}}_{\hat{e}}\|_{\partial \hat{E}}$ is a norm in $\hat{\mathbf{V}}(\hat{E})$. Norms equivalence on the reference element $\hat{E}$ gives

$$\|\hat{\mathbf{v}} \cdot \hat{\mathbf{n}}_{\hat{e}}\|_{\partial \hat{E}} \approx \|\hat{\mathbf{v}}\|_{\hat{E}}, \quad \forall \hat{\mathbf{v}} \in \hat{\mathbf{V}}(\hat{E}).$$

Now, (4.34) follows from (2.7), (2.5), and the scaling estimate (3.15). $\square$

Theorem 4.1. *The velocity* $\mathbf{u}^*_h$ *of the enhanced* $\mathcal{FGM}$ *mixed finite element method* (3.11)–(3.12) *and the postprocessed velocity* $\mathcal{P}(\mathbf{u}_h)$ *of* (4.30)-(4.31) *satisfies*

$$(4.35) \qquad \|\mathbf{u}^*_h - \mathcal{P}(\mathbf{u}_h)\| \lesssim h(|\mathbf{u}|_1 + \|p\|_2).$$

Proof. By Lemma 4.1, there exists $\mathbf{u}^*_{h,0}, \tilde{\mathbf{u}}_{h,0} \in \mathbf{V}^*_{h,0}(E)$ and $\mathbf{u}^*_{h,1}, \tilde{\mathbf{u}}_{h,1} \in \mathbf{V}_h(E)$ such that

$$(4.36) \qquad \mathbf{u}^*_h = \mathbf{u}^*_{h,0} + \mathbf{u}^*_{h,1} \quad \text{and} \quad \tilde{\mathbf{u}}_h = \tilde{\mathbf{u}}_{h,0} + \tilde{\mathbf{u}}_{h,1}.$$

Taking $\mathbf{v}|_E \in \mathbf{V}^*_{h,0}(E)$, $\mathbf{v} = 0$ on $\Omega \setminus E$ in (3.11) gives

$$(4.37) \qquad (K^{-1}\mathbf{u}^*_h, \mathbf{v})_E = 0, \quad \forall \mathbf{v} \in \mathbf{V}^*_{h,0}(E).$$

Subtracting (4.32) from this equation yields

(4.38) $$(K^{-1}(\mathbf{u}_h^* - \tilde{\mathbf{u}}_h), \mathbf{v})_E = 0, \quad \forall \mathbf{v} \in \mathbf{V}_{h,0}^*(E)$$

Taking $\mathbf{v} = \mathbf{u}_{h,0}^* - \tilde{\mathbf{u}}_{h,0} \in \mathbf{V}_{h,0}^*(E)$ in (4.38), we have that

(4.39)
$$\|\mathbf{u}_{h,0}^* - \tilde{\mathbf{u}}_{h,0}\|_E^2 \lesssim (K^{-1}(\mathbf{u}_{h,0}^* - \tilde{\mathbf{u}}_{h,0}), \mathbf{u}_{h,0}^* - \tilde{\mathbf{u}}_{h,0})_E$$
$$= -(K^{-1}(\mathbf{u}_{h,1}^* - \tilde{\mathbf{u}}_{h,1}), \mathbf{u}_{h,0}^* - \tilde{\mathbf{u}}_{h,0})_E \lesssim \|\mathbf{u}_{h,1}^* - \tilde{\mathbf{u}}_{h,1}\|_E \|\mathbf{u}_{h,0}^* - \tilde{\mathbf{u}}_{h,0}\|_E.$$

This implies

(4.40) $$\|\mathbf{u}_h^* - \tilde{\mathbf{u}}_h\|_E \leq \|\mathbf{u}_{h,0}^* - \tilde{\mathbf{u}}_{h,0}\|_E + \|\mathbf{u}_{h,1}^* - \tilde{\mathbf{u}}_{h,1}\|_E \lesssim \|\mathbf{u}_{h,1}^* - \tilde{\mathbf{u}}_{h,1}\|_E,$$

thus it is enough to estimate $\|\mathbf{u}_{h,1}^* - \tilde{\mathbf{u}}_{h,1}\|_E$. Since $\mathbf{u}_{h,1}^* - \tilde{\mathbf{u}}_{h,1} \in \mathbf{V}_h(E)$, Lemma 4.2 gives, for all $e \in \partial E$,

(4.41)
$$\|\mathbf{u}_{h,1}^* - \tilde{\mathbf{u}}_{h,1}\|_E \lesssim h^{1/2}\|(\mathbf{u}_{h,1}^* - \tilde{\mathbf{u}}_{h,1}) \cdot \mathbf{n}_e\|_e = h^{1/2}\|(\mathbf{u}_h^* - \mathbf{u}_h) \cdot \mathbf{n}_e\|_e$$
$$\leq h^{1/2}\|(\mathbf{u} - \mathbf{u}_h^*) \cdot \mathbf{n}_e\|_e + h^{1/2}\|(\mathbf{u} - \mathbf{u}_h) \cdot \mathbf{n}_e\|_e,$$

where we used the fact that on any face e, $\mathbf{u}_{h,1}^* \cdot \mathbf{n}_e = \mathbf{u}_h^* \cdot \mathbf{n}_e$ and $\tilde{\mathbf{u}}_{h,1} \cdot \mathbf{n}_e = \tilde{\mathbf{u}}_h \cdot \mathbf{n}_e = \mathbf{u}_h \cdot \mathbf{n}_e$ in the equality. A combination of (4.40), (4.41), Theorem 3.2, and Theorem 2.2 completes the proof. □

Theorem 4.2. *The postprocessed velocity* $\mathcal{P}(\mathbf{u}_h)$ *of* (4.30)-(4.31) *satisfies*

(4.42) $$\|\mathbf{u} - \mathcal{P}(\mathbf{u}_h)\| \lesssim h(|\mathbf{u}|_1 + \|p\|_2).$$

Proof. The assertion of the theorem follows from (3.13), Theorem 4.1, and

$$\|\mathbf{u} - \mathcal{P}(\mathbf{u}_h)\| \leq \|\mathbf{u} - \mathbf{u}_h^*\| + \|\mathbf{u}_h^* - \mathcal{P}(\mathbf{u}_h)\|.$$

□

5. Numerical experiments

We solve the problem (2.1)–(2.2) with a given analytical solution

$$p(x, y, z) = \sin(\pi x) \sin(\pi y) \sin(\pi z)$$

and a full permeability tensor

$$\mathbf{K} = \begin{pmatrix} 3 & 2.5 & 2.1 \\ 2.5 & 5 & 3.2 \\ 2.1 & 3.2 & 4 \end{pmatrix}.$$

We consider three hexahedral meshes as shown in Figure 3. The first mesh is an h-perturbed grid given in [27]. The second mesh is generated by randomly perturbing positions of vertices in a uniform cubic mesh. More precisely, the new grid points are determined by

$$x_{\text{new}} = x_{\text{old}} + \eta_1 h, \ y_{\text{new}} = y_{\text{old}} + \eta_2 h, \ z_{\text{new}} = z_{\text{old}} + \eta_3 h,$$

where $x_{\text{old}}, y_{\text{old}}, z_{\text{old}}$ are the uniform mesh points, h is the mesh size of the uniform mesh, and η_i (i=1,2,3) are random numbers between -0.25 and 0.25. The third mesh is an h-perturbed fishbone-like mesh from [18]. The first mesh gives planar faces and the others give non-planar faces.

In Table 1, we test the convergence of the enhanced $\mathcal{BDDF}_1$ and enhanced $\mathcal{FGM}$ interpolations. Both $\|\mathbf{u} - \Pi\mathbf{u}\|$ and $\|\mathbf{u} - \Pi^*\mathbf{u}\|$ are approximated by the 27-point Gaussian quadrature rule on the reference cube. On the first mesh, $\|\mathbf{u} - \Pi\mathbf{u}\|$ has first order convergence, but the convergence on the second and third meshes
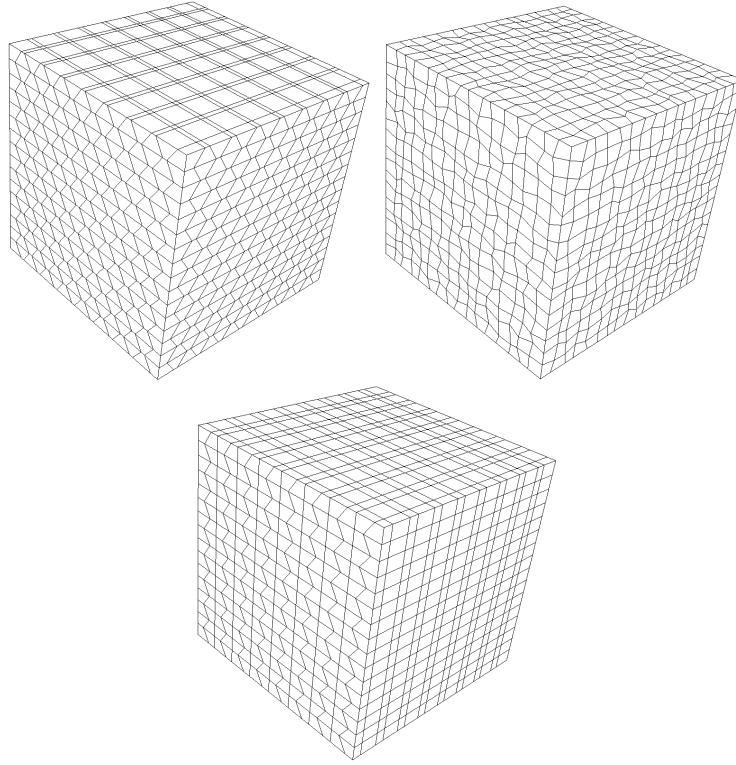
FIGURE 3. Mesh 1: an h-perturbed mesh [27] (top-left); Mesh 2: a randomly h-perturbed hexahedral mesh (top-right); and Mesh 3: an h-perturbed mesh [18] (bottom).

deteriorates. As Lemma 3.2 predicts, $\|\mathbf{u} - \Pi^*\mathbf{u}\|$ has first order convergence on all three meshes.

Table 2 shows the convergence of both the original MFMFE and the postprocessed solution. The error in the face velocities is measured in the norm

$$\|\mathbf{v}\|^2_{\mathcal{F}_h} := \sum_{E \in \mathcal{T}_h} \sum_{e \in \partial E} \frac{|E|}{|e|} \|\mathbf{v} \cdot \mathbf{n}_e\|^2_e.$$

The L^2 norm on the face e is calculated with the 9 point Gaussian quadrature rule on the reference square. Other L^2 norms such as $\|p - p_h\|$, $\|\mathbf{u} - \mathbf{u}_h\|$, and $\|\mathbf{u} - \mathcal{P}(\mathbf{u}_h)\|$ are approximated by the 27-point Gaussian quadrature rule on the reference cube. As predicted by Theorem 2.2, it is first order convergent on all meshes. Due to the first order convergence of the interpolant on the first mesh, we do get first order convergence for the original and postprocessed velocity. On the second and third meshes, the convergence of $\|\mathbf{u} - \mathbf{u}_h\|$ deteriorates, while the postprocessed velocity $\mathcal{P}(\mathbf{u}_h)$ has first order convergence, as Theorem 4.2 predicts.

6. Conclusions

A velocity postprocessing of face fluxes computed using the multipoint flux mixed finite element has been introduced. The algorithm involves first using the MFMFE for computing fluxes on faces followed by solving a 3×3 system on each element. The latter involves utilizing an enhancement of the mixed finite element space introduced

TABLE 1. Convergence of interpolation

$$\|\mathbf{u} - \Pi\mathbf{u}\|$$

$1/h$	Mesh 1		Mesh 2		Mesh 3	
4	3.21E+00		1.93E+00		2.20E+00	
8	1.62E+00	0.99	6.16E-01	1.65	7.77E-01	1.50
16	8.33E-01	0.96	2.77E-01	1.15	3.77E-01	1.04
32	4.25E-01	0.97	1.95E-01	0.51	2.63E-01	0.52
64	2.15E-01	0.98	1.74E-01	0.16	2.32E-01	0.18
128	1.08E-01	0.99	1.69E-01	0.04	2.23E-01	0.06

$$\|\mathbf{u} - \Pi^*\mathbf{u}\|$$

$1/h$	Mesh 1		Mesh 2		Mesh 3	
4	2.99E+00		1.89E+00		2.12E+00	
8	1.42E+00	1.07	5.75E-01	1.72	7.09E-01	1.58
16	7.04E-01	1.01	2.12E-01	1.44	2.85E-01	1.31
32	3.54E-01	0.99	9.56E-02	1.15	1.32E-01	1.11
64	1.78E-01	0.99	4.60E-02	1.05	6.48E-02	1.02
128	8.90E-02	1.00	2.28E-02	1.01	3.22E-02	1.01

by Falk, Gatto, and Monk [18]. The resulting postprocessed velocities are shown to be first order. Computational results verifying the theory are presented.

Appendix   Basis functions for the new finite elements

A.1   Basis functions for the enhanced $\mathcal{BDDF}_1$ space. Recall that in the MFMFE method, equivalent DOF are chosen leading to a cell-centered stencil for the pressure. Let $\hat{\mathbf{v}} := (\hat{v}_1, \hat{v}_2, \hat{v}_3)^T \in \hat{\mathbf{V}}(\hat{E})$ and denote the DOF as

On the face $\hat{x} = 0$: $\mathcal{N}_1(\hat{\mathbf{v}}) := \hat{v}_1(0,0,0),$ $\mathcal{N}_2(\hat{\mathbf{v}}) := \hat{v}_1(0,1,0),$

$\mathcal{N}_3(\hat{\mathbf{v}}) := \hat{v}_1(0,1,1),$ $\mathcal{N}_4(\hat{\mathbf{v}}) := \hat{v}_1(0,0,1),$

On the face $\hat{x} = 0$: $\mathcal{N}_5(\hat{\mathbf{v}}) := \hat{v}_1(1,0,0),$ $\mathcal{N}_6(\hat{\mathbf{v}}) := \hat{v}_1(1,1,0),$

$\mathcal{N}_7(\hat{\mathbf{v}}) := \hat{v}_1(1,1,1),$ $\mathcal{N}_8(\hat{\mathbf{v}}) := \hat{v}_1(1,0,1),$

On the face $\hat{y} = 0$: $\mathcal{N}_9(\hat{\mathbf{v}}) := \hat{v}_2(0,0,0),$ $\mathcal{N}_{10}(\hat{\mathbf{v}}) := \hat{v}_2(1,0,0),$

$\mathcal{N}_{11}(\hat{\mathbf{v}}) := \hat{v}_2(1,0,1),$ $\mathcal{N}_{12}(\hat{\mathbf{v}}) := \hat{v}_2(0,0,1),$

On the face $\hat{y} = 1$: $\mathcal{N}_{13}(\hat{\mathbf{v}}) := \hat{v}_2(0,1,0),$ $\mathcal{N}_{14}(\hat{\mathbf{v}}) := \hat{v}_2(1,1,0),$

$\mathcal{N}_{15}(\hat{\mathbf{v}}) := \hat{v}_2(1,1,1),$ $\mathcal{N}_{16}(\hat{\mathbf{v}}) := \hat{v}_2(0,1,1),$

On the face $\hat{z} = 0$: $\mathcal{N}_{17}(\hat{\mathbf{v}}) := \hat{v}_3(0,0,0),$ $\mathcal{N}_{18}(\hat{\mathbf{v}}) := \hat{v}_3(1,0,0),$

$\mathcal{N}_{19}(\hat{\mathbf{v}}) := \hat{v}_3(1,1,0),$ $\mathcal{N}_{20}(\hat{\mathbf{v}}) := \hat{v}_3(0,1,0),$

On the face $\hat{z} = 1$: $\mathcal{N}_{21}(\hat{\mathbf{v}}) := \hat{v}_3(0,0,1),$ $\mathcal{N}_{22}(\hat{\mathbf{v}}) := \hat{v}_3(1,0,1),$

$\mathcal{N}_{23}(\hat{\mathbf{v}}) := \hat{v}_3(1,1,1),$ $\mathcal{N}_{24}(\hat{\mathbf{v}}) := \hat{v}_3(0,1,1).$

Let the corresponding 24 nodal basis functions of $\hat{V}(\hat{E})$ be $\hat{\mathbf{v}}_i$ $(i = 1, \ldots 24)$, i.e.,

$$\mathcal{N}_j(\hat{\mathbf{v}}_i) = \delta_{ij}, \quad j = 1, \ldots, 24,$$

where δ_{ij} is the delta function. Solving the above equation gives the 24 basis functions.

TABLE 2. Convergence of solution

Mesh 1

$1/h$	$\|p - p_h\|$		$\|\mathbf{u} - \mathbf{u}_h\|_{\mathcal{F}_h}$		$\|\mathbf{u} - \mathbf{u}_h\|$		$\|\mathbf{u} - \mathcal{P}(\mathbf{u}_h)\|$	
4	2.74E-01		3.89E+00		3.39E+00		3.39E+00	
8	1.51E-01	0.86	1.81E+00	1.10	1.73E+00	0.97	1.73E+00	0.97
16	7.93E-02	0.93	8.82E-01	1.04	8.79E-01	0.98	8.79E-01	0.98
32	4.05E-02	0.97	4.39E-01	1.01	4.44E-01	0.99	4.44E-01	0.99
64	2.05E-02	0.98	2.19E-01	1.00	2.24E-01	0.99	2.24E-01	0.99
128	1.03E-02	0.99	1.10E-01	0.99	1.12E-01	1.00	1.12E-01	1.00

Mesh 2

$1/h$	$\|p - p_h\|$		$\|\mathbf{u} - \mathbf{u}_h\|_{\mathcal{F}_h}$		$\|\mathbf{u} - \mathbf{u}_h\|$		$\|\mathbf{u} - \mathcal{P}(\mathbf{u}_h)\|$	
4	2.56E-01		3.56E+00		2.49E+00		2.47E+00	
8	1.27E-01	1.01	1.35E+00	1.40	1.07E+00	1.22	1.05E+00	1.23
16	6.41E-02	0.98	6.04E-01	1.16	5.23E-01	1.03	4.96E-01	1.08
32	3.22E-02	0.99	3.53E-01	0.77	2.97E-01	0.82	2.46E-01	1.01
64	1.61E-02	1.00	1.68E-01	1.07	2.07E-01	0.52	1.23E-01	1.00
128	8.07E-03	1.00	8.77E-02	0.94	1.79E-01	0.21	6.21E-02	0.99

Mesh 3

$1/h$	$\|p - p_h\|$		$\|\mathbf{u} - \mathbf{u}_h\|_{\mathcal{F}_h}$		$\|\mathbf{u} - \mathbf{u}_h\|$		$\|\mathbf{u} - \mathcal{P}(\mathbf{u}_h)\|$	
4	2.73E-01		4.26E+00		2.76E+00		2.73E+00	
8	1.35E-01	1.02	1.74E+00	1.29	1.20E+00	1.20	1.18E+00	1.21
16	6.72E-02	1.00	7.92E-01	1.14	5.92E-01	1.02	5.46E-01	1.11
32	3.36E-02	1.00	3.83E-01	1.05	3.47E-01	0.77	2.66E-01	1.04
64	1.68E-02	1.00	1.89E-01	1.02	2.57E-01	0.43	1.32E-01	1.01
128	8.39E-03	1.00	9.43E-02	1.00	2.30E-01	0.16	6.57E-02	1.01

On the face $x = 0$:

$$\hat{\mathbf{v}}_1 = [xy - y - z - x + xz + yz - xyz + 1, \;\; y/4 - y^2/4, \;\; z/2 - yz/2 + yz^2/2 - z^2/2]^T,$$
$$\hat{\mathbf{v}}_2 = [y - xy - yz + xyz, \;\; y^2/4 - y/4, \;\; yz/2 - yz^2/2]^T,$$
$$\hat{\mathbf{v}}_3 = [yz - xyz, \;\; y^2/4 - y/4, \;\; yz^2/2 - yz/2]^T,$$
$$\hat{\mathbf{v}}_4 = [z - xz - yz + xyz, \;\; y/4 - y^2/4, \;\; yz/2 - z/2 - yz^2/2 + z^2/2]^T.$$

On the face $x = 1$:

$$\hat{\mathbf{v}}_5 = [x - xy - xz + xyz, \;\; y^2/4 - y/4, \;\; yz/2 - z/2 - yz^2/2 + z^2/2]^T,$$
$$\hat{\mathbf{v}}_6 = [xy - xyz, \;\; y/4 - y^2/4, \;\; yz^2/2 - yz/2]^T,$$
$$\hat{\mathbf{v}}_7 = [xyz, \;\; y/4 - y^2/4, \;\; yz/2 - yz^2/2]^T,$$
$$\hat{\mathbf{v}}_8 = [xz - xyz, \;\; y^2/4 - y/4, \;\; z/2 - yz/2 + yz^2/2 - z^2/2]^T.$$

On the face $y = 0$:

$$\hat{\mathbf{v}}_9 = [x/2 - xz/2 + x^2z/2 - x^2/2, \ \ xy - y - z - x + xz + yz - xyz + 1, \ \ z/4 - z^2/4]^T,$$
$$\hat{\mathbf{v}}_{10} = [xz/2 - x/2 - x^2z/2 + x^2/2, \ \ x - xy - xz + xyz, \ \ z/4 - z^2/4]^T,$$
$$\hat{\mathbf{v}}_{11} = [x^2z/2 - xz/2, \ \ xz - xyz, \ \ z^2/4 - z/4]^T,$$
$$\hat{\mathbf{v}}_{12} = [xz/2 - x^2z/2, \ \ z - xz - yz + xyz, \ \ z^2/4 - z/4]^T.$$

On the face $y = 1$:

$$\hat{\mathbf{v}}_{13} = [xz/2 - x/2 - x^2z/2 + x^2/2, \ \ y - xy - yz + xyz, \ \ z^2/4 - z/4]^T,$$
$$\hat{\mathbf{v}}_{14} = [x/2 - xz/2 + x^2z/2 - x^2/2, \ \ xy - xyz, \ \ z^2/4 - z/4]^T,$$
$$\hat{\mathbf{v}}_{15} = [xz/2 - x^2z/2, \ \ xyz, \ \ z/4 - z^2/4]^T,$$
$$\hat{\mathbf{v}}_{16} = [x^2z/2 - xz/2, \ \ yz - xyz, \ \ z/4 - z^2/4]^T.$$

On the face $z = 0$:

$$\hat{\mathbf{v}}_{17} = [x/4 - x^2/4, \ \ y/2 - xy/2 + xy^2/2 - y^2/2, \ \ xy - y - z - x + xz + yz - xyz + 1]^T,$$
$$\hat{\mathbf{v}}_{18} = [x^2/4 - x/4, \ \ xy/2 - xy^2/2, \ \ x - xy - xz + xyz]^T,$$
$$\hat{\mathbf{v}}_{19} = [x^2/4 - x/4, \ \ xy^2/2 - xy/2, \ \ xy - xyz]^T,$$
$$\hat{\mathbf{v}}_{20} = [x/4 - x^2/4, \ \ xy/2 - y/2 - xy^2/2 + y^2/2, \ \ y - xy - yz + xyz]^T.$$

On the face $z = 1$:

$$\hat{\mathbf{v}}_{21} = [x^2/4 - x/4, \ \ xy/2 - y/2 - xy^2/2 + y^2/2, \ \ z - xz - yz + xyz]^T,$$
$$\hat{\mathbf{v}}_{22} = [x/4 - x^2/4, \ \ xy^2/2 - xy/2, \ \ xz - xyz]^T,$$
$$\hat{\mathbf{v}}_{23} = [x/4 - x^2/4, \ \ xy/2 - xy^2/2, \ \ xyz]^T,$$
$$\hat{\mathbf{v}}_{24} = [x^2/4 - x/4, \ \ y/2 - xy/2 + xy^2/2 - y^2/2, \ \ yz - xyz]^T.$$

A.2   Basis functions for the enhanced $\mathcal{F}\mathcal{G}\mathcal{M}$ space. Define three additional DOF for the space $\hat{\mathbf{V}}^*(\hat{E})$

$$\mathcal{N}_{25}(\hat{\mathbf{v}}) := (\hat{\mathbf{v}}, \hat{\mathbf{r}}_1)_{\hat{E}}, \quad \mathcal{N}_{26}(\hat{\mathbf{v}}) := (\hat{\mathbf{v}}, \hat{\mathbf{r}}_2)_{\hat{E}}, \quad \mathcal{N}_{27}(\hat{\mathbf{v}}) := (\hat{\mathbf{v}}, \hat{\mathbf{r}}_3)_{\hat{E}}.$$

The 27 nodal basis functions $\mathbf{v}_i^*$ $(i = 1, \ldots, 27)$ of $\hat{\mathbf{V}}^*(\hat{E})$ are found by solving

$$\mathcal{N}_j(\mathbf{v}_i^*) = \delta_{ij}, \quad j = 1, \ldots, 27.$$

On the face $x = 0$:

$$\hat{\mathbf{v}}_1^* = \begin{bmatrix} 7xy/4 - y - z - 7x/4 + 7xz/4 + yz - 3x^2y/4 - 3x^2z/4 + 3x^2/4 - xyz + 1 \\ 3y/4 - 3xy/4 - yz/4 + 3xy^2/4 + y^2z/4 - 3y^2/4 \\ 3z/4 - 3xz/4 - yz/4 + 3xz^2/4 + yz^2/4 - 3z^2/4 \end{bmatrix},$$

$$\hat{\mathbf{v}}_2^* = \begin{bmatrix} y - 7xy/4 + 3xz/4 - yz + 3x^2y/4 - 3x^2z/4 + xyz \\ 3xy/4 - 3y/4 + yz/4 - 3xy^2/4 - y^2z/4 + 3y^2/4 \\ z/2 - 3xz/4 + yz/4 + 3xz^2/4 - yz^2/4 - z^2/2 \end{bmatrix},$$

$$\hat{\mathbf{v}}_3^* = \begin{bmatrix} 3x/4 - 3xy/4 - 3xz/4 + yz + 3x^2y/4 + 3x^2z/4 - 3x^2/4 - xyz \\ 3xy/4 - y/2 - yz/4 - 3xy^2/4 + y^2z/4 + y^2/2 \\ 3xz/4 - z/2 - yz/4 - 3xz^2/4 + yz^2/4 + z^2/2 \end{bmatrix},$$

$$\hat{\mathbf{v}}_4^* = \begin{bmatrix} z + 3xy/4 - 7xz/4 - yz - 3x^2y/4 + 3x^2z/4 + xyz \\ y/2 - 3xy/4 + yz/4 + 3xy^2/4 - y^2z/4 - y^2/2 \\ 3xz/4 - 3z/4 + yz/4 - 3xz^2/4 - yz^2/4 + 3z^2/4 \end{bmatrix}.$$

On the face $x = 1$:

$$\hat{\mathbf{v}}_5^* = \begin{bmatrix} x/4 - xy/4 - xz/4 - 3x^2y/4 - 3x^2z/4 + 3x^2/4 + xyz \\ yz/4 - 3xy/4 + 3xy^2/4 - y^2z/4 \\ yz/4 - 3xz/4 + 3xz^2/4 - yz^2/4 \end{bmatrix},$$

$$\hat{\mathbf{v}}_6^* = \begin{bmatrix} xy/4 + 3xz/4 + 3x^2y/4 - 3x^2z/4 - xyz \\ 3xy/4 - yz/4 - 3xy^2/4 + y^2z/4 \\ z/4 - 3xz/4 - yz/4 + 3xz^2/4 + yz^2/4 - z^2/4 \end{bmatrix},$$

$$\hat{\mathbf{v}}_7^* = \begin{bmatrix} 3x/4 - 3xy/4 - 3xz/4 + 3x^2y/4 + 3x^2z/4 - 3x^2/4 + xyz \\ 3xy/4 - y/4 + yz/4 - 3xy^2/4 - y^2z/4 + y^2/4 \\ 3xz/4 - z/4 + yz/4 - 3xz^2/4 - yz^2/4 + z^2/4 \end{bmatrix},$$

$$\hat{\mathbf{v}}_8^* = \begin{bmatrix} 3xy/4 + xz/4 - 3x^2y/4 + 3x^2z/4 - xyz \\ y/4 - 3xy/4 - yz/4 + 3xy^2/4 + y^2z/4 - y^2/4 \\ 3xz/4 - yz/4 - 3xz^2/4 + yz^2/4 \end{bmatrix}.$$

On the face $y = 0$:

$$\hat{\mathbf{v}}_9^* = \begin{bmatrix} 3x/4 - 3xy/4 - xz/4 + 3x^2y/4 + x^2z/4 - 3x^2/4 \\ 7xy/4 - 7y/4 - z - x + xz + 7yz/4 - 3xy^2/4 - 3y^2z/4 + 3y^2/4 - xyz + 1 \\ 3z/4 - xz/4 - 3yz/4 + xz^2/4 + 3yz^2/4 - 3z^2/4 \end{bmatrix},$$

$$\hat{\mathbf{v}}_{10}^* = \begin{bmatrix} 3xy/4 - 3x/4 + xz/4 - 3x^2y/4 - x^2z/4 + 3x^2/4 \\ x - 7xy/4 - xz + 3yz/4 + 3xy^2/4 - 3y^2z/4 + xyz \\ z/2 + xz/4 - 3yz/4 - xz^2/4 + 3yz^2/4 - z^2/2 \end{bmatrix},$$

$$\hat{\mathbf{v}}_{11}^* = \begin{bmatrix} 3xy/4 - x/2 - xz/4 - 3x^2y/4 + x^2z/4 + x^2/2 \\ 3y/4 - 3xy/4 + xz - 3yz/4 + 3xy^2/4 + 3y^2z/4 - 3y^2/4 - xyz \\ 3yz/4 - xz/4 - z/2 + xz^2/4 - 3yz^2/4 + z^2/2 \end{bmatrix},$$

$$\hat{\mathbf{v}}_{12}^* = \begin{bmatrix} x/2 - 3xy/4 + xz/4 + 3x^2y/4 - x^2z/4 - x^2/2 \\ z + 3xy/4 - xz - 7yz/4 - 3xy^2/4 + 3y^2z/4 + xyz \\ xz/4 - 3z/4 + 3yz/4 - xz^2/4 - 3yz^2/4 + 3z^2/4 \end{bmatrix}.$$

On the face $y = 1$:

$$\hat{\mathbf{v}}_{13}^* = \begin{bmatrix} xz/4 - 3xy/4 + 3x^2y/4 - x^2z/4 \\ y/4 - xy/4 - yz/4 - 3xy^2/4 - 3y^2z/4 + 3y^2/4 + xyz \\ xz/4 - 3yz/4 - xz^2/4 + 3yz^2/4 \end{bmatrix},$$

$$\hat{\mathbf{v}}_{14}^* = \begin{bmatrix} 3xy/4 - xz/4 - 3x^2y/4 + x^2z/4 \\ xy/4 + 3yz/4 + 3xy^2/4 - 3y^2z/4 - xyz \\ z/4 - xz/4 - 3yz/4 + xz^2/4 + 3yz^2/4 - z^2/4 \end{bmatrix},$$

$$\hat{\mathbf{v}}_{15}^* = \begin{bmatrix} 3xy/4 - x/4 + xz/4 - 3x^2y/4 - x^2z/4 + x^2/4 \\ 3y/4 - 3xy/4 - 3yz/4 + 3xy^2/4 + 3y^2z/4 - 3y^2/4 + xyz \\ xz/4 - z/4 + 3yz/4 - xz^2/4 - 3yz^2/4 + z^2/4 \end{bmatrix},$$

$$\hat{\mathbf{v}}_{16}^* = \begin{bmatrix} x/4 - 3xy/4 - xz/4 + 3x^2y/4 + x^2z/4 - x^2/4 \\ 3xy/4 + yz/4 - 3xy^2/4 + 3y^2z/4 - xyz \\ 3yz/4 - xz/4 + xz^2/4 \end{bmatrix}.$$

On the face $z = 0$:

$$\hat{\mathbf{v}}_{17}^* = \begin{bmatrix} 3x/4 - xy/4 - 3xz/4 + x^2y/4 + 3x^2z/4 - 3x^2/4 \\ 3y/4 - xy/4 - 3yz/4 + xy^2/4 + 3y^2z/4 - 3y^2/4 \\ xy - y - 7z/4 - x + 7xz/4 + 7yz/4 - 3xz^2/4 - 3yz^2/4 + 3z^2/4 - xyz + 1 \end{bmatrix},$$

$$\hat{\mathbf{v}}_{18}^* = \begin{bmatrix} xy/4 - 3x/4 + 3xz/4 - x^2y/4 - 3x^2z/4 + 3x^2/4 \\ y/2 + xy/4 - 3yz/4 - xy^2/4 + 3y^2z/4 - y^2/2 \\ x - xy - 7xz/4 + 3yz/4 + 3xz^2/4 - 3yz^2/4 + xyz \end{bmatrix},$$

$$\hat{\mathbf{v}}_{19}^* = \begin{bmatrix} 3xz/4 - xy/4 - x/2 + x^2y/4 - 3x^2z/4 + x^2/2 \\ 3yz/4 - xy/4 - y/2 + xy^2/4 - 3y^2z/4 + y^2/2 \\ 3z/4 + xy - 3xz/4 - 3yz/4 + 3xz^2/4 + 3yz^2/4 - 3z^2/4 - xyz \end{bmatrix},$$

$$\hat{\mathbf{v}}_{20}^* = \begin{bmatrix} x/2 + xy/4 - 3xz/4 - x^2y/4 + 3x^2z/4 - x^2/2 \\ xy/4 - 3y/4 + 3yz/4 - xy^2/4 - 3y^2z/4 + 3y^2/4 \\ y - xy + 3xz/4 - 7yz/4 - 3xz^2/4 + 3yz^2/4 + xyz \end{bmatrix}.$$

On the face $z = 1$:

$$\hat{\mathbf{v}}_{21}^* = \begin{bmatrix} xy/4 - 3xz/4 - x^2y/4 + 3x^2z/4 \\ xy/4 - 3yz/4 - xy^2/4 + 3y^2z/4 \\ z/4 - xz/4 - yz/4 - 3xz^2/4 - 3yz^2/4 + 3z^2/4 + xyz \end{bmatrix},$$

$$\hat{\mathbf{v}}_{22}^* = \begin{bmatrix} 3xz/4 - xy/4 + x^2y/4 - 3x^2z/4 \\ y/4 - xy/4 - 3yz/4 + xy^2/4 + 3y^2z/4 - y^2/4 \\ xz/4 + 3yz/4 + 3xz^2/4 - 3yz^2/4 - xyz \end{bmatrix},$$

$$\hat{\mathbf{v}}_{23}^* = \begin{bmatrix} xy/4 - x/4 + 3xz/4 - x^2y/4 - 3x^2z/4 + x^2/4 \\ xy/4 - y/4 + 3yz/4 - xy^2/4 - 3y^2z/4 + y^2/4 \\ 3z/4 - 3xz/4 - 3yz/4 + 3xz^2/4 + 3yz^2/4 - 3z^2/4 + xyz \end{bmatrix},$$

$$\hat{\mathbf{v}}_{24}^* = \begin{bmatrix} x/4 - xy/4 - 3xz/4 + x^2y/4 + 3x^2z/4 - x^2/4 \\ -xy/4 + 3yz/4 + xy^2/4 - 3y^2z/4 \\ 3xz/4 + yz/4 - 3xz^2/4 + 3yz^2/4 - xyz \end{bmatrix}.$$

Additional three DOF inside the element:

$$\hat{\mathbf{v}}_{25}^* = \begin{bmatrix} 0 \\ 18y - 36yz + 36y^2z - 18y^2 \\ 36yz - 18z - 36yz^2 + 18z^2 \end{bmatrix},$$

$$\hat{\mathbf{v}}_{26}^* = \begin{bmatrix} 18x - 36xz + 36x^2z - 18x^2 \\ 0 \\ 36xz - 18z - 36xz^2 + 18z^2 \end{bmatrix},$$

$$\hat{\mathbf{v}}_{27}^* = \begin{bmatrix} 18x - 36xy + 36x^2y - 18x^2 \\ 36xy - 18y - 36xy^2 + 18y^2 \\ 0 \end{bmatrix}.$$

A.3 Local postprocessing. Write the MFMFE solution on the reference element $\hat{E}$ as

$$\hat{\mathbf{u}}_h = \sum_{i=1}^{24} \hat{u}_i \hat{\mathbf{v}}_i.$$

Since the MFMFE and the enhanced $\mathcal{FGM}$ spaces have the same face DOF, the postprocessed velocity on the reference element can be written as

$$\widehat{\mathcal{P}(\mathbf{u}_h)} = \sum_{i=1}^{24} \hat{u}_i \hat{\mathbf{v}}_i^* + \hat{u}_{25} \hat{\mathbf{v}}_{25}^* + \hat{u}_{26} \hat{\mathbf{v}}_{26}^* + \hat{u}_{27} \hat{\mathbf{v}}_{27}^*.$$

Let

$$\mathcal{K}_E^{-1} := \frac{1}{J} DF_E^T K^{-1} DF_E.$$

Then $\hat{u}_{25}$, $\hat{u}_{26}$, and $\hat{u}_{27}$ is the solution of the following 3 by 3 system:

$$\begin{pmatrix} (\mathcal{K}_E^{-1}\hat{\mathbf{v}}_{25}^*, \hat{\mathbf{v}}_{25}^*)_{\hat{E}} & (\mathcal{K}_E^{-1}\hat{\mathbf{v}}_{26}^*, \hat{\mathbf{v}}_{25}^*)_{\hat{E}} & (\mathcal{K}_E^{-1}\hat{\mathbf{v}}_{27}^*, \hat{\mathbf{v}}_{25}^*)_{\hat{E}} \\ (\mathcal{K}_E^{-1}\hat{\mathbf{v}}_{25}^*, \hat{\mathbf{v}}_{26}^*)_{\hat{E}} & (\mathcal{K}_E^{-1}\hat{\mathbf{v}}_{26}^*, \hat{\mathbf{v}}_{26}^*)_{\hat{E}} & (\mathcal{K}_E^{-1}\hat{\mathbf{v}}_{27}^*, \hat{\mathbf{v}}_{26}^*)_{\hat{E}} \\ (\mathcal{K}_E^{-1}\hat{\mathbf{v}}_{25}^*, \hat{\mathbf{v}}_{27}^*)_{\hat{E}} & (\mathcal{K}_E^{-1}\hat{\mathbf{v}}_{26}^*, \hat{\mathbf{v}}_{27}^*)_{\hat{E}} & (\mathcal{K}_E^{-1}\hat{\mathbf{v}}_{27}^*, \hat{\mathbf{v}}_{27}^*)_{\hat{E}} \end{pmatrix} \begin{pmatrix} \hat{u}_{25} \\ \hat{u}_{26} \\ \hat{u}_{27} \end{pmatrix}$$

$$= - \begin{pmatrix} \sum_{i=1}^{24} (\mathcal{K}_E^{-1}\hat{\mathbf{v}}_i^*, \hat{\mathbf{v}}_{25}^*)_{\hat{E}} \hat{u}_i \\ \sum_{i=1}^{24} (\mathcal{K}_E^{-1}\hat{\mathbf{v}}_i^*, \hat{\mathbf{v}}_{26}^*)_{\hat{E}} \hat{u}_i \\ \sum_{i=1}^{24} (\mathcal{K}_E^{-1}\hat{\mathbf{v}}_i^*, \hat{\mathbf{v}}_{27}^*)_{\hat{E}} \hat{u}_i \end{pmatrix}.$$

References

[1] I. AAVATSMARK, *An introduction to multipoint flux approximations for quadrilateral grids*, Comp. Geosci., 6 (2002), pp. 405–432.

[2] I. AAVATSMARK, T. BARKVE, O. BOE, AND T. MANNSETH, *Discretization on unstructured grids for inhomogeneous, anisotropic media. Part II: Discussion and numerical results*, SIAM J. Sci. Comput., 19 (1998), pp. 1717–1736.

[3] I. AAVATSMARK, G. T. EIGESTAD, R. A. KLAUSEN, M. F. WHEELER, AND I. YOTOV, *Convergence of a symmetric MPFA method on quadrilateral grids*, Computational Geosciences, 11 (2007), pp. 333–345.

[4] S. AGMON, *Lectures on Elliptic Boundary Value Problems*, Van Nostrand, Princeton, NJ, 1965.

[5] D. N. ARNOLD, *An interior penalty finite element method with discontinuous elements*, SIAM J. Numer. Anal., 19 (1982), pp. 742–760.

[6] D. N. ARNOLD, D. BOFFI, AND R. S. FALK, *Quadrilateral H(div) finite elements*, SIAM J. Numer. Anal., 42 (2005), pp. 2429–2451.

[7] F. BREZZI, J. DOUGLAS, R. DURAN, AND M. FORTIN, *Mixed finite elements for second order elliptic problems in three variables*, Numer. Math., 51 (1987), pp. 237–250.

[8] F. BREZZI, J. DOUGLAS, AND L. D. MARINI, *Two families of mixed finite elements for second order elliptic problems*, Numer. Math., 47 (1985), pp. 217–235.

[9] F. BREZZI AND M. FORTIN, *Mixed and Hybrid Finite Element Methods*, Spring-Verlag, New York, 1991.

[10] F. BREZZI, K. LIPNIKOV, AND M. SHASHKOV, *Convergence of mimetic finite difference method for diffusion problems on polyhedral meshes*, SIAM J. Numer. Anal., 43 (2005), pp. 1872–1896.

[11] Z. CHEN AND J. DOUGLAS, *Prismatic mixed finite elements for second order elliptic problems*, Calcolo, 26 (1989), pp. 135–148.

[12] P. G. CIARLET, *The Finite Element Method for Elliptic Problems*, Stud. Math. Appl. 4, North-Holland, Amsterdam, 1978; reprinted, SIAM, Philadelphia, 2002.

[13] H. K. DAHLE, M. S. ESPEDAL, AND O. SÆVAREID, *Characteristic, local grid refinement techniques for reservoir flow problems*, International Journal for Numerical Methods in Engineering, 34 (1992), pp. 1051–1069.

[14] M. G. EDWARDS, *Unstructured control-volume distributed, full-tensor finite-volume schemes with flow based grids*, Comp. Geosci., 6 (2002), pp. 433–452.

[15] M. G. EDWARDS AND C. F. ROGERS, *Finite volume discretization with imposed flux continuity for the general tensor pressure equation*, Comp. Geosci., 2 (1998), pp. 259–290.

[16] M. S. ESPEDAL, R. E. WING, AND T. F. RUSSELL, *Mixed methods, operator splitting, and local refinement techniques for simulation on irregular grids*, 2nd European Conference on the Mathematics of Oil Recovery, (1990).

[17] R. E. EWING, M. M. LIU, AND J. WANG, *Superconvergence of mixed finite element approximations over quadrilaterals*, SIAM. J. Numer. Anal., 36 (1999), pp. 772–787.

[18] R. S. FALK, P. GATTO, AND P. MONK, *Hexahedral H(div) and H(curl) finite elements*, Mathematical Modeling and Numerical Analysis, 45 (2011), pp. 115–143.

[19] J. HYMAN, M. SHASHKOV, AND S. STEINBERG, *The numerical solution of diffusion problem in strongly heterogeneous non-isotropic materials*, J. Comp. Phys., 132 (1997), pp. 130–148.

[20] R. INGRAM, M. WHEELER, AND I. YOTOV, *A multipoint flux mixed finite element method on hexahedra*, SIAM J. Numer. Anal., 48 (2010), pp. 1281–1312.

[21] R. A. KLAUSEN AND R. WINTHER, *Convergence of multipoint flux approximations on quadri-lateral grids*, Numer. Methods Partial Differential Equations, 22 (2006), pp. 1438–1454.

[22] R. A. KLAUSEN AND R. WINTHER, *Robust convergence of multi point flux approximation on rough grids*, Numer. Math., 104 (2006), pp. 317–337.

[23] Y. KUZNETSOV AND S. REPIN, *Convergence analysis and error estimates for mixed finite element method on distorted meshes*, J. Numer. Math., 13 (2005), pp. 33–51.

[24] K. LIPNIKOV, M. SHASHKOV, AND I. YOTOV, *Local flux mimetic finite difference methods*, Numer. Math., 112 (2009), pp. 115–152.

[25] R. NAFF, T. RUSSELL, AND J. D. WILSON, *Shape functions for velocity interpolation in general hexahedral cells*, Comp. Geosci., 6 (2002), pp. 285–314.

[26] J. M. NORDBOTTEN AND H. HÆGLAND, *On reproducing uniform flow exactly on general hexahedral cells using one degree of freedom per surface*, Advances in Water Resources, 32 (2009), pp. 264–267.

[27] A. SBOUI, J. JAFFRE, AND J. ROBERTS, *A composite mixed finite elements for hexahedral grids*, SIAM. J. Sci. Comput., 31 (2009), pp. 2623–2645.

[28] M. WHEELER AND G. XUE, *Accurate locally conservative discretizations for modeling multi-phase flow in porous media on general hexahedra grids*, Proceedings of the 11th European Conference on the Mathematics of Oil Recovery- ECMOR XII, EAGE, (2010).

[29] M. WHEELER, G. XUE, AND I. YOTOV, *A multiscale mortar multipoint flux mixed finite element method*, Accepted by Mathematical Modeling and Numerical Analysis, (2011).

[30] ———, *Accurate cell-centered discretizations for modeling multiphase flow in porous me-dia on general hexahedral and simplicial grids*, SPE-141534-PP, SPE Reservoir Simulation Symposium, (2011).

[31] ———, *A family of multipoint flux mixed finite element methods for elliptic problems on general grids*, Procedia Computer Science, 4 (2011), pp. 918–927.

[32] ———, *A multipoint flux mixed finite element method on distorted quadrilaterals and hexa-hedra*, Accepted by Numer. Math., (2011).

[33] ———, *A multipoint flux mixed finite element method on triangular prisms*, Preprint, (2011).

[34] M. WHEELER AND I. YOTOV, *A multipoint flux mixed finite element method*, SIAM. J. Numer. Anal., 44 (2006), pp. 2082–2106.

Center for Subsurface Modeling (CSM), Institute for Computational Engineering and Sciences (ICES), The University of Texas at Austin, Austin, TX 78712
  E-mail: `mfw@ices.utexas.edu`

(CSM), (ICES), The University of Texas at Austin, Austin, TX 78712, (present address: Shell International Exploration and Production Inc. 3737 Bellaire Blvd, Rm 2009, Houston, Texas 77025)
  E-mail: `gxue@ices.utexas.edu`

Department of Mathematics, University of Pittsburgh, Pittsburgh, PA 15260
  E-mail: `yotov@math.pitt.edu`